$NiMnO_x$/TiN/CC electrode with branch-leaf structure: a novel approach to improve the performance of supercapacitors under high mass loading amorphous metal oxides

Huayao Tu,[a] *Dong Shi,*[a] *Zhenyan Liang,*[a] *Hehe Jiang,*[a] *Zhen Kong,*[a] *Kang Zang,*[a] *Yongliang Shao,**[a,b] *Yongzhong Wu*[a,b] *and Xiaopeng Hao**[a,b]

a State Key Laboratory of Crystal Materials, Shandong University, Jinan, Shandong, 250100, P. R. China

b Department of Materials Science and Engineering, Qilu University of Technology, Jinan, 250353, P. R. China.

E-mail: shaoyonliang@qlu.edu.cn, xphao@sdu.edu.cn

This file includes:

S1. Chemicals

$MnSO_4 \cdot H_2O$, $KMnO_4$, $NiC_4H_6O_4 \cdot 4H_2O$, tetrabutyl titanate (TBT), acetone (C_3H_6O), $FeCl_3 \cdot 6H_2O$, Na_2SO_4, HCl, and ethanol were purchased from Sinopharm Chemical Reagent Co., Ltd. (Shanghai). All those reagents were analytical grade. NH_3, Ar was purchased from Deyang Special Gas Co., Ltd. (Jinan, China).

S2. Synthetic Methods

Preparation of acid-treated carbon fiber: In a typical procedure, a piece of carbon fiber cloth (1.5 cm× 4 cm) was subsequently cleaned with deionized (DI) water and ethanol under ultrasonic, and dried in an oven. Then, the freshly cleaned CC was added into a stainless-steel autoclave (100 mL) containing commercially available concentrated HNO_3 (50 mL) and DI water (15 mL), and was held at 120 °C for 12 h. Then, the resulted CC was washed thoroughly with DI water until the pH is close to 7.

Synthesis of TiN nanowires: First, a piece of carbon cloth (1.5 cm × 4 cm) was placed in a 100 mL beaker containing 60 mL ethanol and 1mL tetrabutyl titanate and ultrasonic agitation for 1 h. Then the carbon cloth was placed in a muffle furnace and kept at 400℃ for 0.5 h to obtain a carbon cloth with TiO_2 crystal seeds. Next, 15 mL of concentrated hydrochloric acid and 15 mL of acetone were put into a 50 mL beaker and stirred for 0.5 h. Then, 1.5 mL of t tetrabutyl titanate was added slowly and stirred for 1h. Afterward, the solution was transferred into a 50 mL Teflon lined stainless steel autoclave and the carbon cloth with TiO_2 crystal seeds was immersed in the reaction solution. The autoclave liners were kept at 200 °C for 1.5 h and then the obtained TiO_2

array growth on the CC was washed with deionized water, ethanol and dried at 80 °C. TiN/CC nanowires samples were obtained by further annealing TiO_2/CC precursors in NH_3 atmosphere at a heating rate of 5 °C min^{-1} at 800°C for 4 h. Ar atmosphere was used to protect TiO_2/CC precursors during heating and cooling.

Synthesis of $NiMnO_x$/CC, $NiMn_2O_4$/CC, and $NiMnO_x$/TiN/CC electrode materials: First, 0.1 mmol $MnSO_4 \cdot H_2O$ and 0.3 mmol $KMnO_4$ were dissolved in two beakers containing 15 mL of deionized water respectively and stirred for 0.5 h. Next, mix the solutions in the two beakers and continue to stir for 0.5 h. Then, 0.2 mmol $NiC_4H_6O_4 \cdot 4H_2O$ was added into the beaker and continued to be stirred for 0.5 h. Transfer the above solution to a 50 mL Teflon lined stainless steel autoclave. Then, TiN/CC was immersed in the reaction solution. The autoclave was kept at 140 °C for 8 h, then the products were washed with deionized water and ethanol, and dried at 50°C to obtain the $NiMnO_x$/TiN/CC electrode material. In the above process, replace TiN/CC with CC to obtain $NiMnO_x$/CC electrode materials. The $NiMnO_x$/CC electrode materials were further thermally annealed at 450°C under Ar atmosphere for 2 h at the heating rate of 5 °C min^{-1} to obtain $NiMn_2O_4$/CC electrode materials. Furthermore, the amount of added Ni source and Mn source was increased to improve the mass load of $NiMnO_x$ nanosheets in the electrode material. The mass loading of the electrode material was determined by the mass difference before and after hydrothermal treatment.

Synthesis of FeOOH/CC and FeOOH/TiN/CC electrode materials: First, 0.48 g of $FeCl_3 \cdot 6H_2O$ powder and 0.13 g of Na_2SO_4 powder were dissolved with 30 mL of distilled water and stirred for 0.5 h. After that, the above solution was transferred into a 50 mL Teflon lined stainless steel autoclave and one piece of TiN/CC was immersed into the reaction solution. The autoclave liners were kept at 150 °C for 7 h and then the obtained hydroxide array growth on the carbon fiber was washed with deionized (DI) water, ethanol and dried at 50 °C. Finally, FeOOH/TiN/CC electrode materials were obtained. Moreover, in the above process, replace TiN/CC with CC to obtain FeOOH/CC electrode materials.

Assembling flexible ASC devices: The ASC devices were assembled using $NiMnO_x$/TiN/CC and FeOOH/TiN/CC as electrodes with a separator (filter paper) and PVA/Na_2SO_4 as gel electrolyte. First, the PVA/ Na_2SO_4 gel was synthesized by mixing 6 g of Na_2SO_4 and 9 g of PVA in 60 mL of deionized water. Then heat the mixture at 85°C and stirred vigorously for 2 h. Before assembly, the positive and negative electrodes and diaphragm were immersed in PVA/Na_2SO_4 gel for 5 min to assemble the ASC device and encapsulated by a thermoplastic machine. Finally, the device was maintained at 45 ℃ overnight. The entire as-fabricated device was compact at an area of approximately 7.5 cm^2 (5 cm × 1.5 cm).

S3. Materials Characterization

The morphology and phase structure of the samples were investigated with FESEM (Hitachis-S4800), HRTEM (JEM 2100F), XRD (Bruker D8 Advance), and XPS (Philips Tecnai Twin-20U), respectively.

S4. Electrochemical Tests

The electrochemical characterizations of the prepared electrodes were tested using a three-electrode system on a CHI660E electrochemical workstation (Shanghai Chen Hua Instruments Co., China). In the test system, the self-supported binder-free prepared electrodes were used as the working electrode, with a platinum sheet (1 cm × 1 cm) as a counter electrode and Ag/AgCl as a reference electrode, in a 1.0 M Na_2SO_4 aqueous solution.

All the electrochemical measurements with galvanostatic charge/discharge (GCD), cyclic voltammetry (CV), and electrochemical impedance spectroscopy (EIS) techniques were conducted in a three-electrode system. For detail, CV and GCD curves were collected against SCE by varying the scan rate from 5 mV s^{-1} to 100 mV s^{-1} and current density from 5 to 100 mA cm^{-2}, respectively. Alternating current EIS spectra were collected within a frequency range of 10^{-2} Hz – 10^{5} Hz at the open-circuit voltage with an AC amplitude of 5 mV.

For three-electrode cells, specific capacity derived from GCD discharge curves was calculated as:

$$C(mF/cm^2) = I\int (1/V(t))dt$$

where I is the applied constant-current density, t is the discharge time, and V(t) is the potential as a function of t.

Areal energy density (E, Wh cm^{-2}) and power density (P, W cm^{-2}) of the flexible ASC devices are calculated using the following equations:

$$Es = \frac{Cs \times U^2}{2 \times 3600}$$

$$Ps = \frac{Es \times 3600}{\Delta t}$$

Where Cs (mF cm^{-2}) is the specific capacitance, U is the operating voltage (V), Δt is the discharge time of flexible ASC.

S5. Supplementary Figs. S1–S34

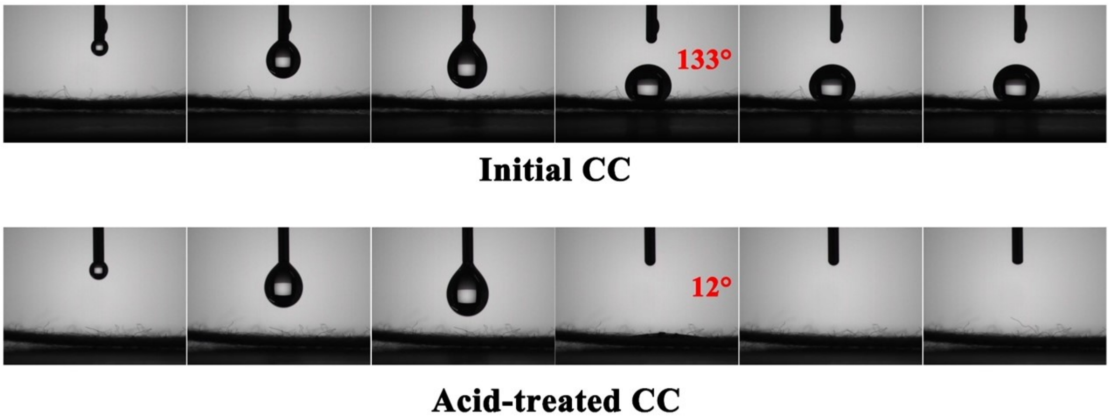

Fig. S1 Water contact angles of CC and acid-treated clean CC

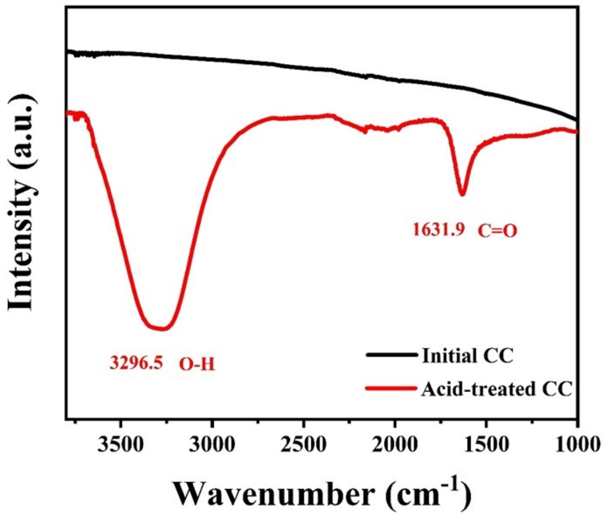

Fig. S2 FTIR spectra of CC and acid-treated clean CC

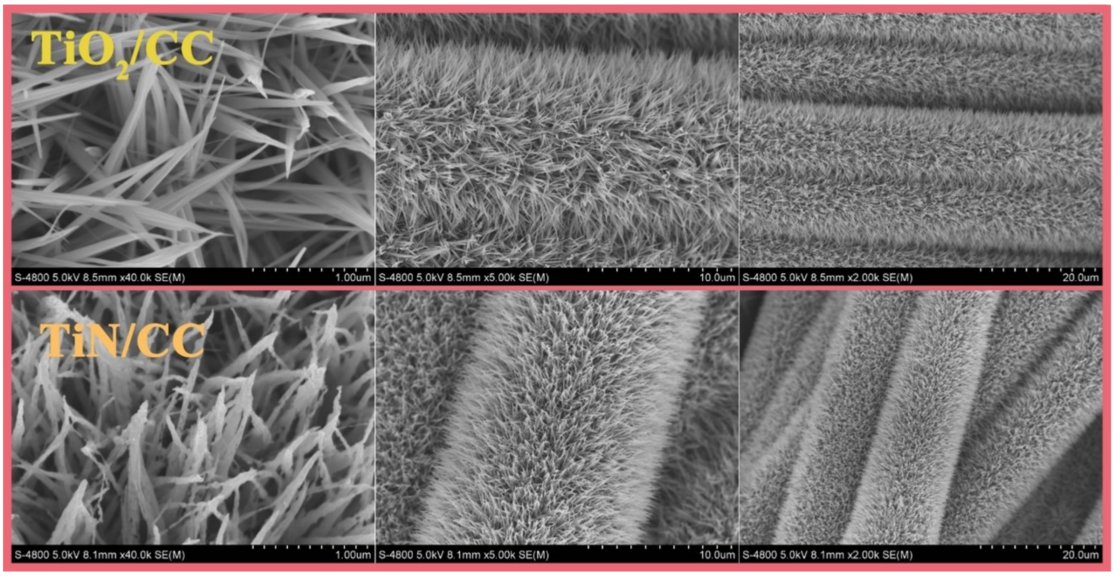

Fig. S3 SEM images of TiO_2 nanowire and TiN nanowire.

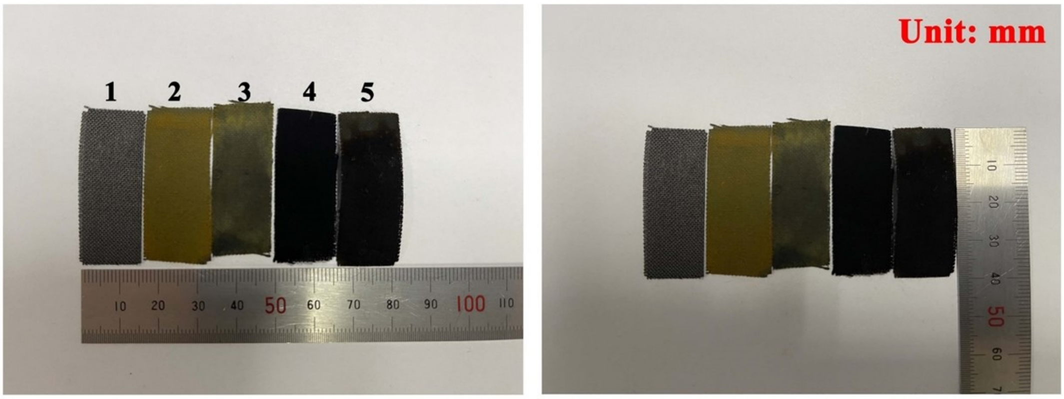

1: CC 2: FeOOH/CC 3: FeOOH/TiN/CC 4: $NiMnO_x$/CC 5: $NiMnO_x$/TiN/CC

Fig. S4 Fig. S4 Digital photos of as-prepared electrode materials

CC (0.298 mm)	**FeOOH/CC (0.339 mm)**	**FeOOH/TiN/CC (0.363 mm)**	**$NiMnO_x$/CC (0.349 mm)**	**$NiMnO_x$/TiN/CC (0.374 mm)**

Fig. S5 The thickness display of the prepared electrode materials

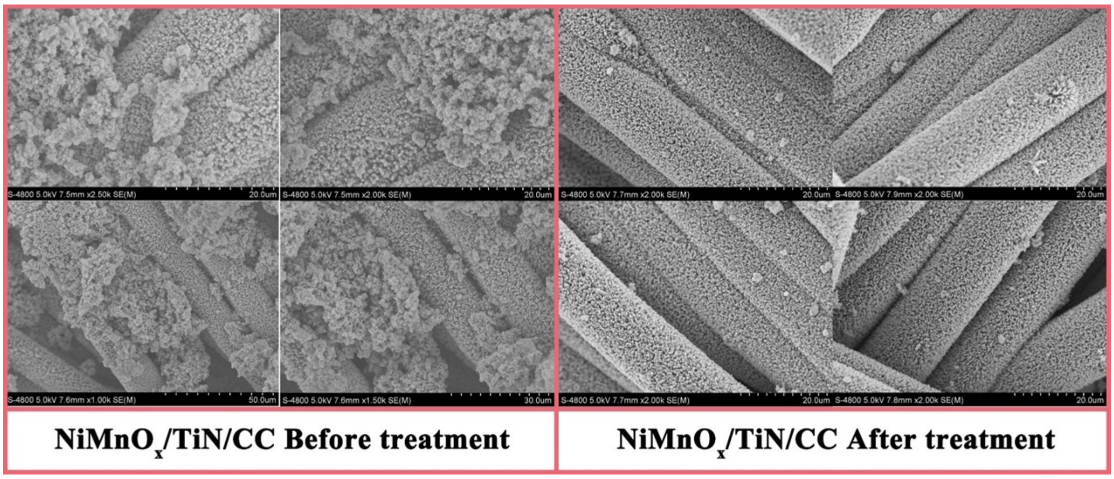

Fig. S6 SEM images of $NiMnO_x/TiN/CC$ electrode materials before and after treatment

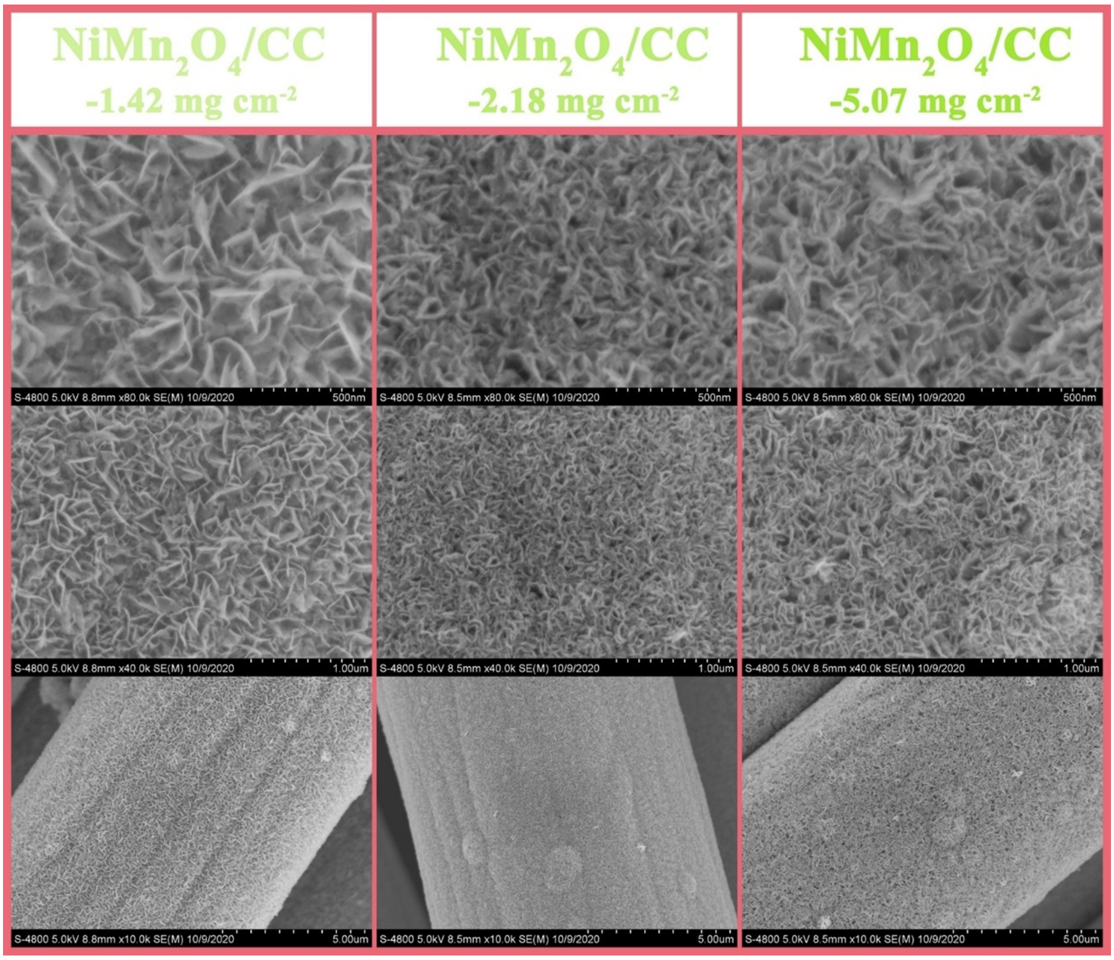

Fig. S7 SEM images of $NiMn_2O_4/CC$ under different mass loading (from 1.42 to 5.07 mg cm^{-2}).

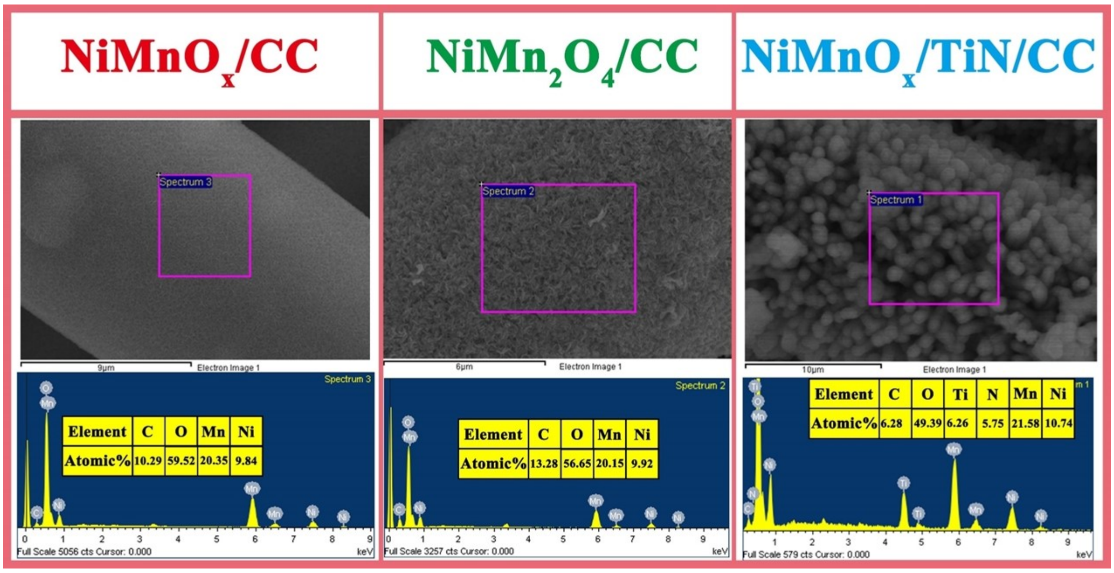

Fig. S8 EDS characterization of $NiMnO_x$/CC, $NiMn_2O_4$/CC, and $NiMnO_x$/TiN/CC electrode materials

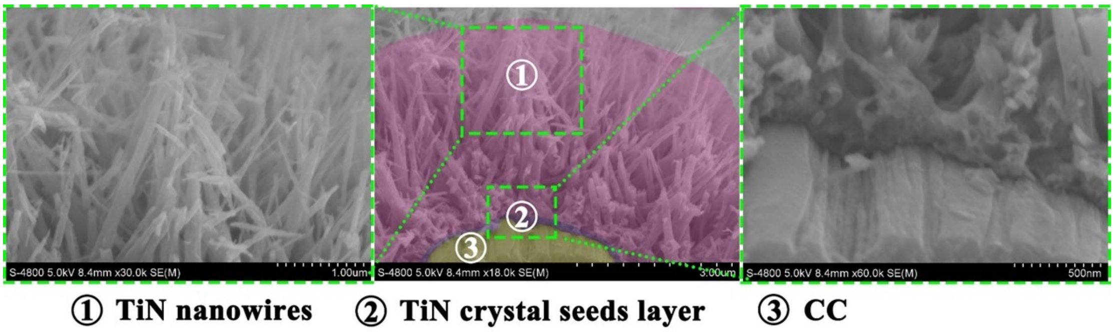

Fig. S9 Cross-section SEM images of TiN/CC electrode material

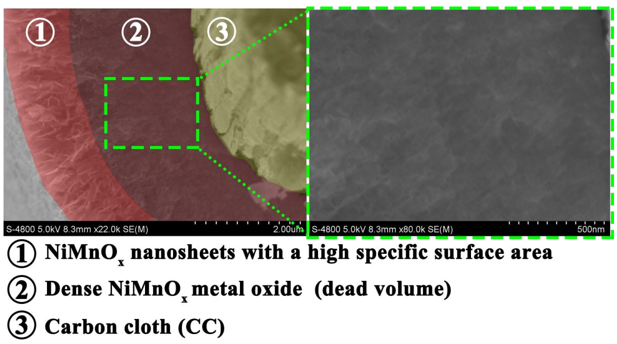

Fig. S10 Cross-section SEM images of $NiMnO_x$/CC electrode material under high mass loading

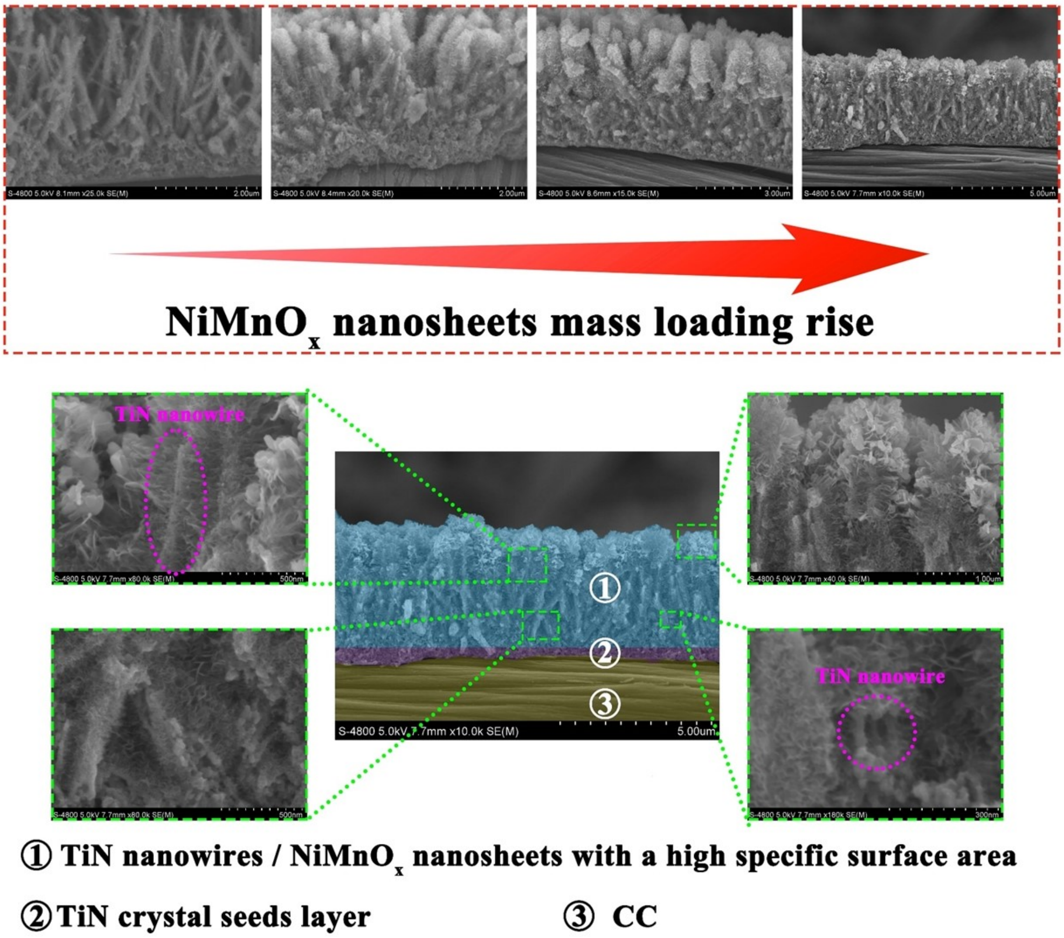

Fig. S11 Cross-section SEM images of $NiMnO_x$/TiN/CC electrode material under different mass loading

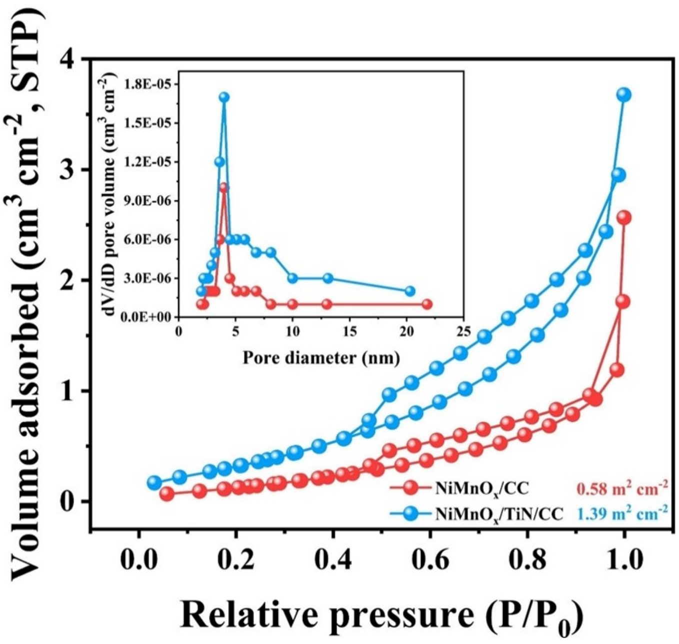

Fig. S12 Nitrogen adsorption–desorption isotherms of $NiMnO_x$/CC and $NiMnO_x$/TiN/CC electrodes.

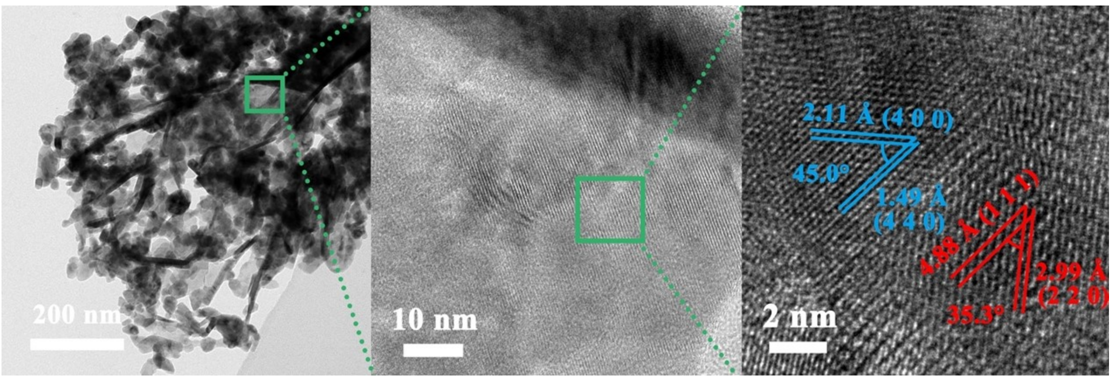

Fig. S13 TEM and HRTEM of $NiMn_2O_4$/CC electrodes.

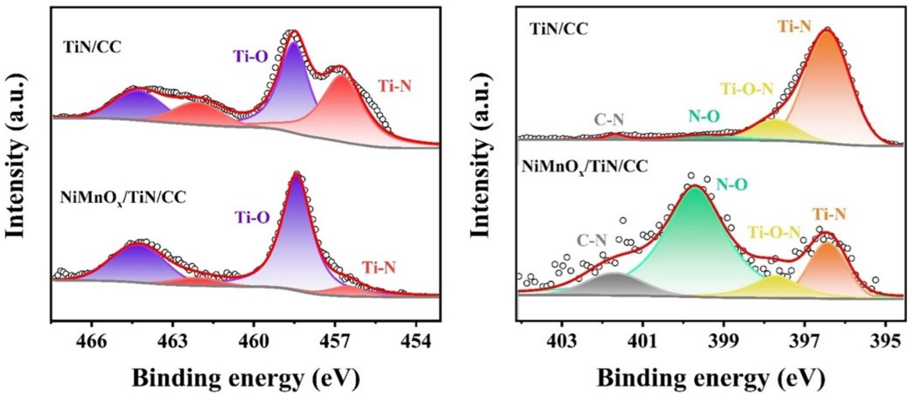

Fig. S14 XPS spectra of Ti 2p and N 1s in TiN/CC and $NiMnO_x$/TiN/CC electrode materials

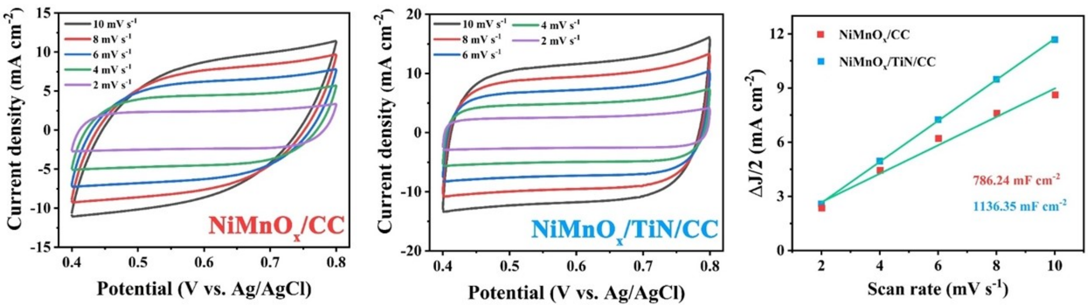

Fig. S15 The electrochemically active area of the prepared $NiMnO_x$/CC and NiMnOx/TiN/CC electrodes were estimated through utilizing a series of CV curves at different scan rates. CV curves at different scan rates in the region between 0.4 V and 0.8 V (vs. SCE) were recorded. The differences in current densities ($\Delta J/2 = (Ja - Jc)/2$ at 0.6 V (vs. SCE) plotted against the scan rates fit to a linear regression and the slope is C_{dl} (double layer capacitance).

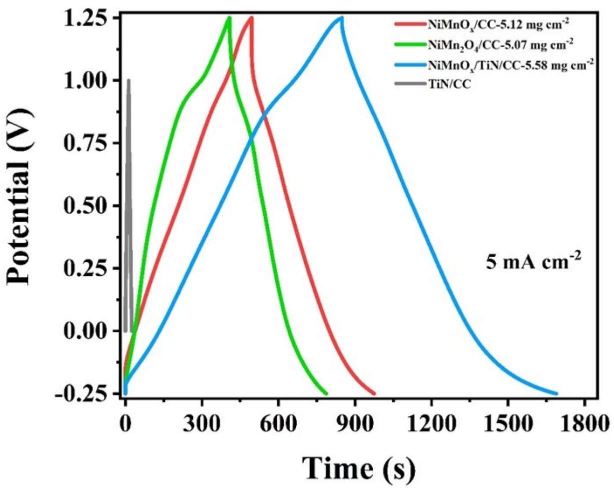

Fig. S16 GCD curves of TiN/CC, $NiMnO_x$/CC, $NiMn_2O_4$/CC and $NiMnO_x$/TiN/CC electrodes at 5 mA cm^{-2}.

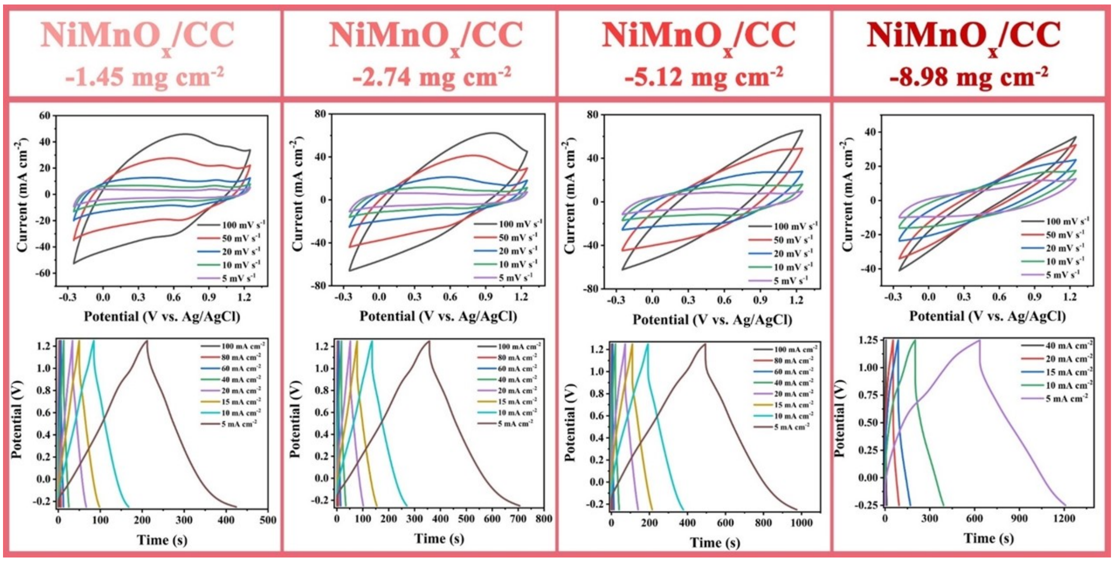

Fig. S17 CV and GCD curves of $NiMnO_x$/CC electrode.

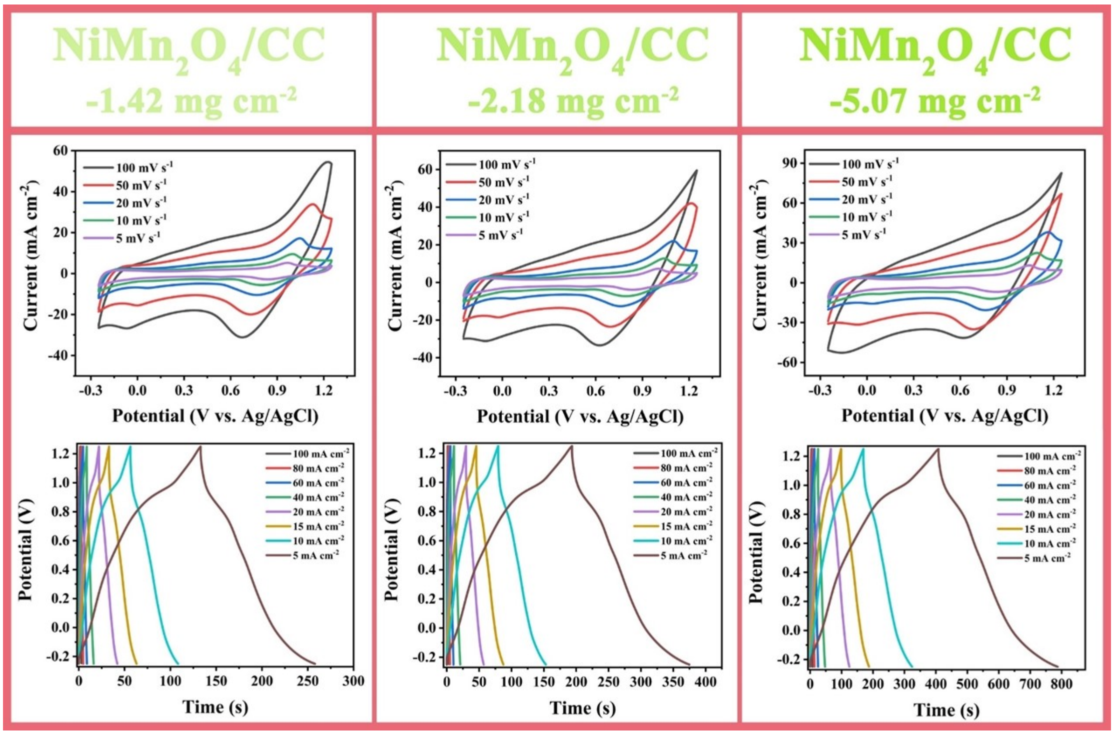

Fig. S18 CV and GCD curves of $NiMn_2O_4$/CC electrode.

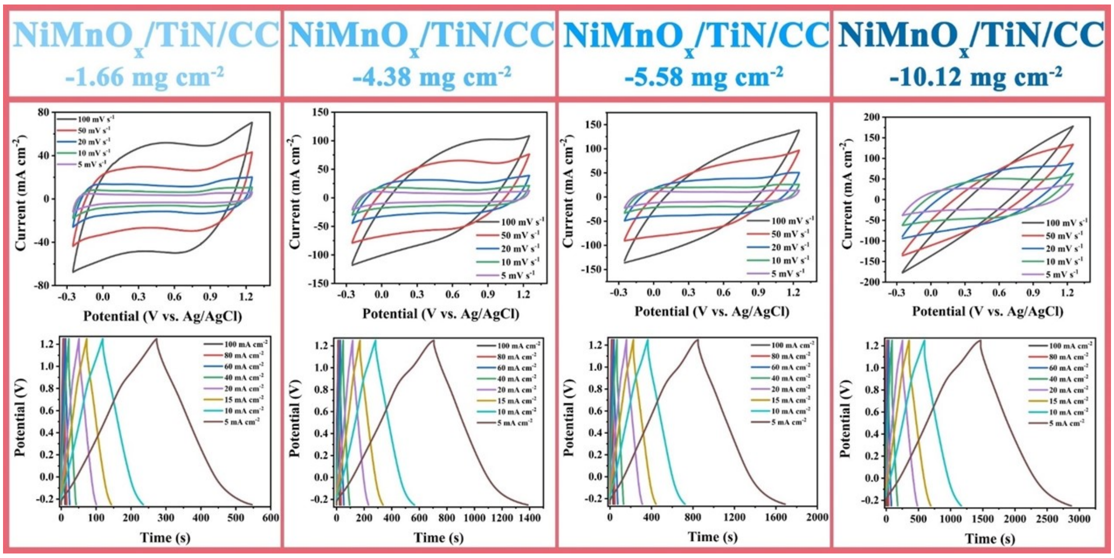

Fig. S19 CV and GCD curves of $NiMnO_x$/TiN/CC electrode.

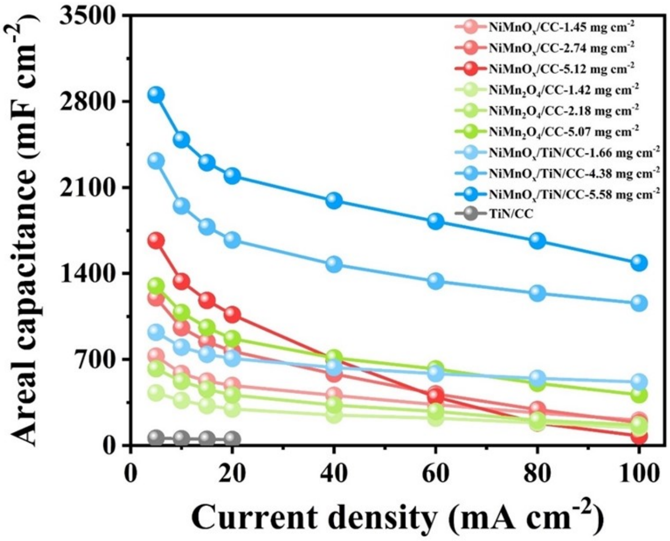

Fig. S20 Rate performance of NiMnO$_x$/CC, NiMn$_2$O$_4$/CC and NiMnO$_x$/TiN/CC electrodes (mass loading from 1.42 to 5.58 mg cm^{-2}).

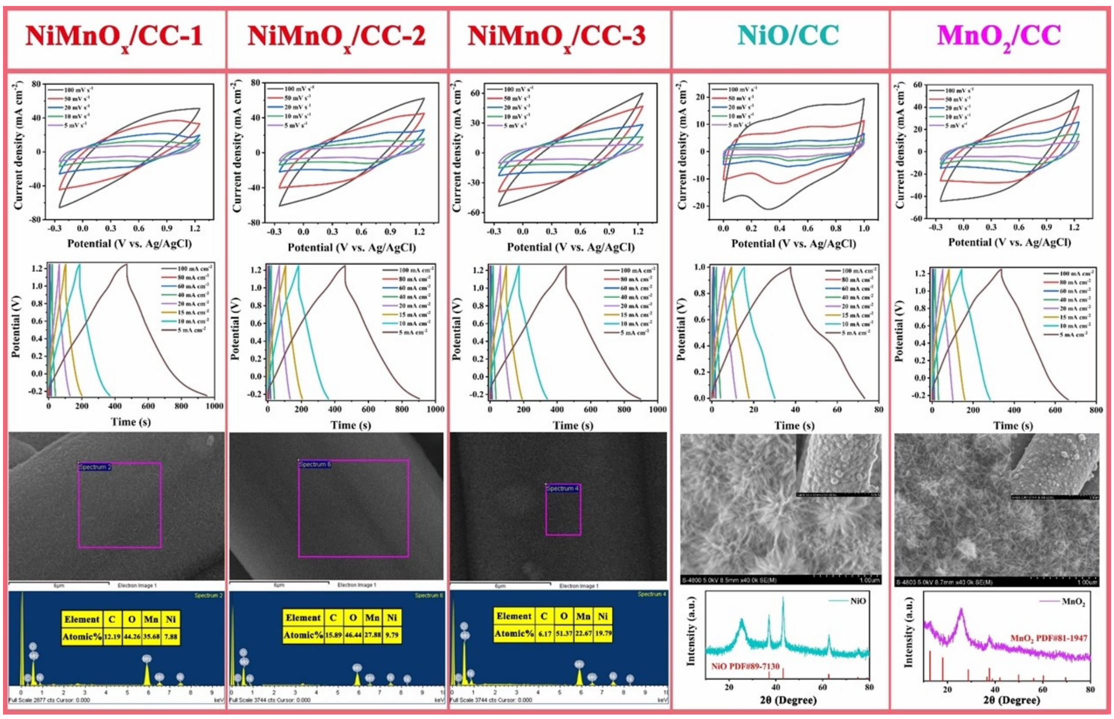

Fig. S21 The electrochemical performances of NiO, MnO$_2$, and NiMnO$_x$/CC electrode materials with different atomic ratios of Ni to Mn (1:4.53, 1:2.85, 1.15:1) under same mass loading (about 5 mg cm^{-2})

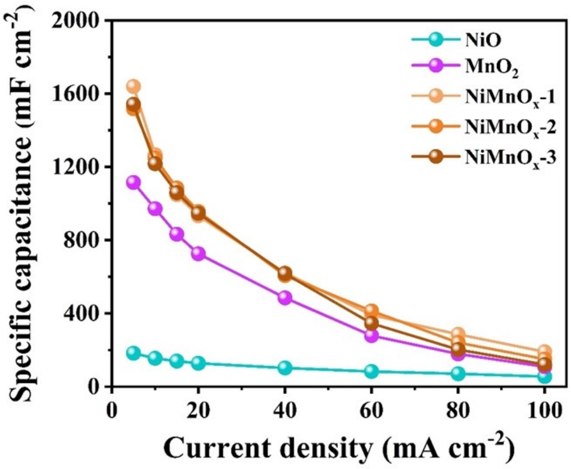

Fig. S22 Rate performances of NiO, MnO_2, and $NiMnO_x$/CC electrode materials with different atomic ratios of Ni to Mn

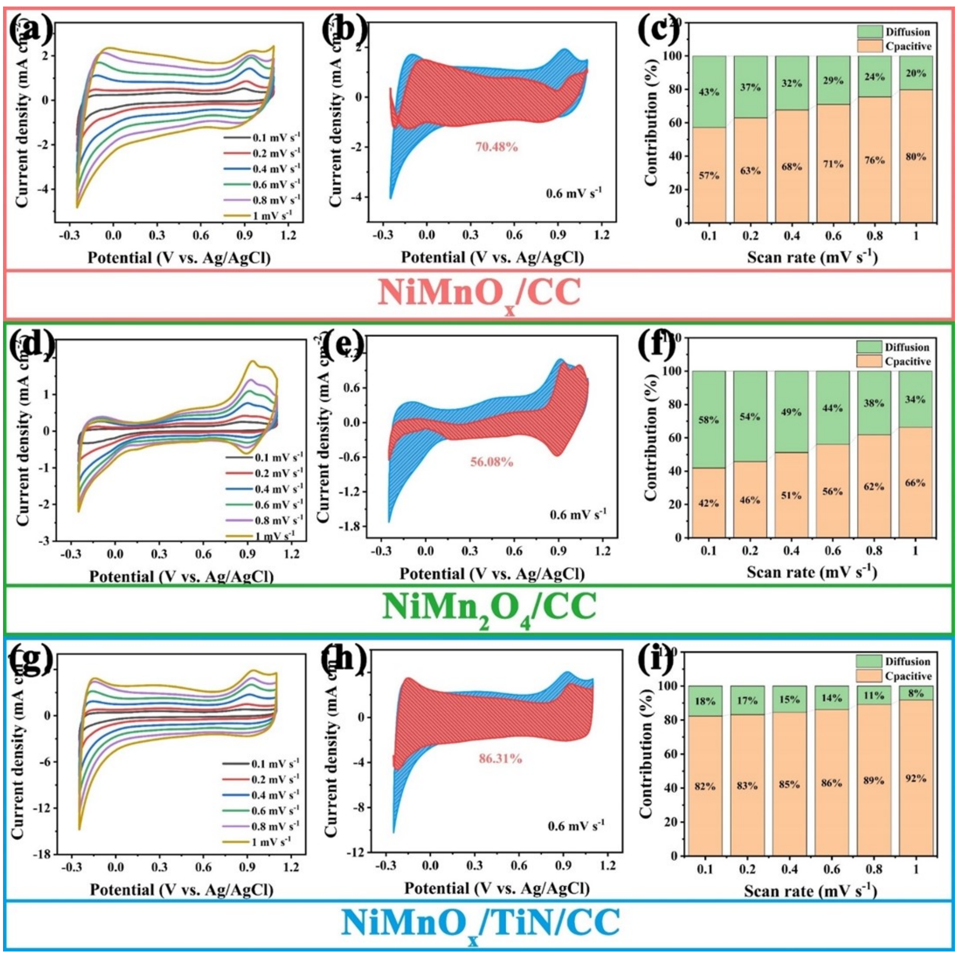

Fig. S23 Analysis of dynamic process for $NiMnO_x$/CC, $NiMn_2O_4$/CC and

NiMnO$_x$/TiN/CC materials: (a, d, g) CV curves at scan rate of 0.1 to 1 mV s^{-1}, (b, e, h) Proportion of capacitive current and diffusion current at 0.6 mV s^{-1}, (c, f, i) Histogram of capacitive behavior contribution at different scan rates.

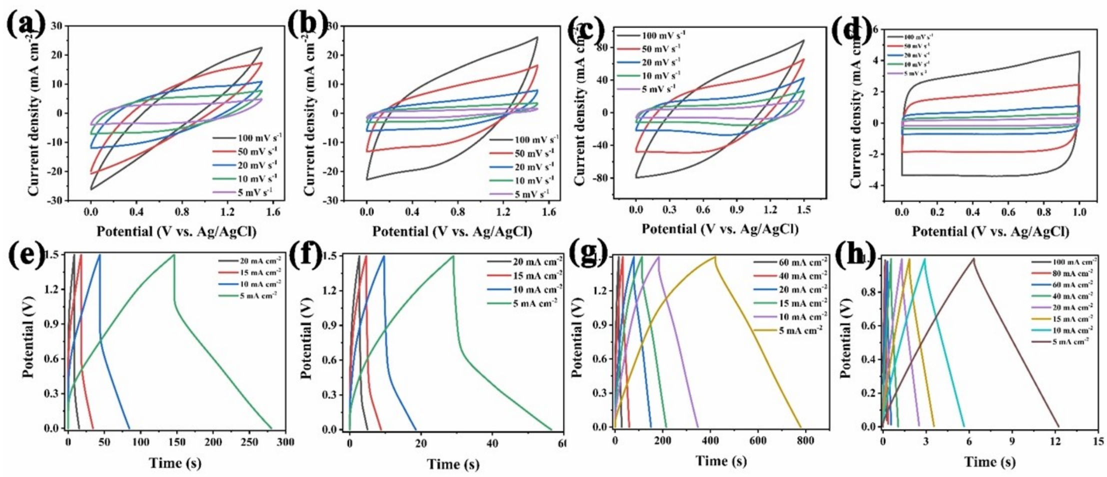

Fig. S24 CV and GCD curves of symmetric supercapacitor devices: (a, e) NiMnO$_x$/CC, (b, f) NiMn$_2$O$_4$/CC, (c, g) NiMnO$_x$/TiN/CC, (d, h) TiN/CC.

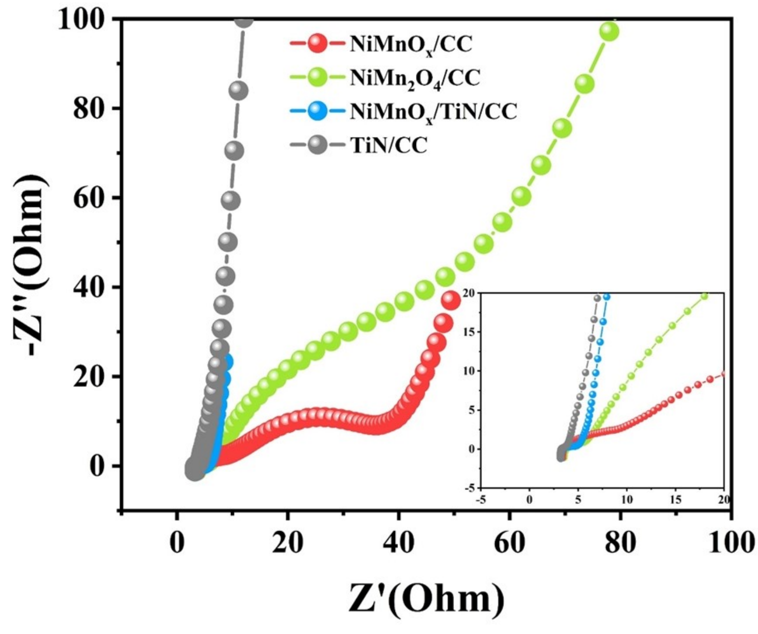

Fig. S25 Nyquist plots of NiMnO$_x$/CC, NiMn$_2$O$_4$/CC and NiMnO$_x$/TiN/CC symmetric supercapacitor devices.

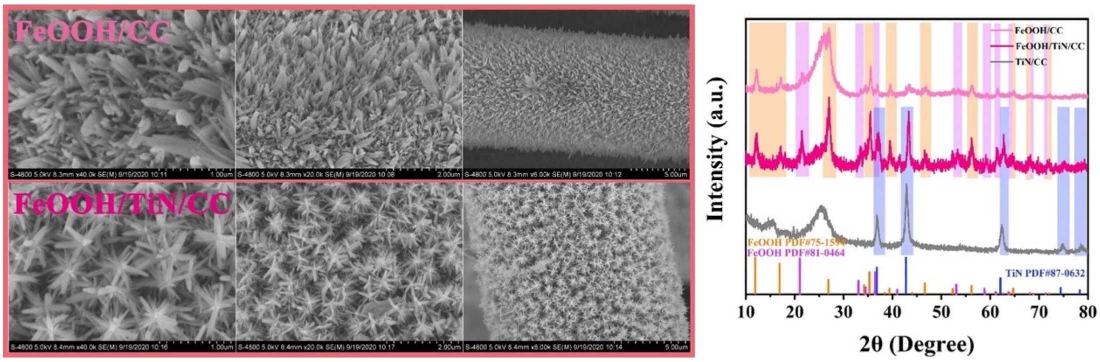

Fig. S26 SEM images and XRD patterns of FeOOH/CC and FeOOH/TiN/CC electrodes.

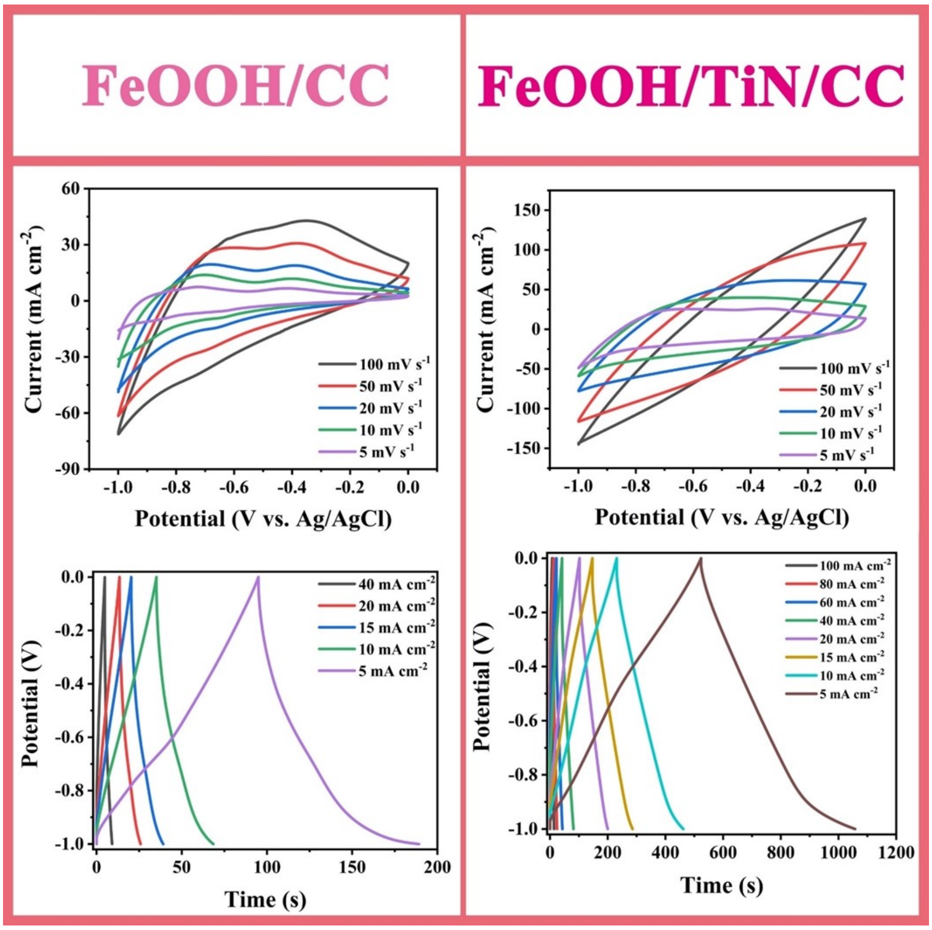

Fig. S27 CV and GCD curves of FeOOH/CC and FeOOH/TiN/CC electrodes.

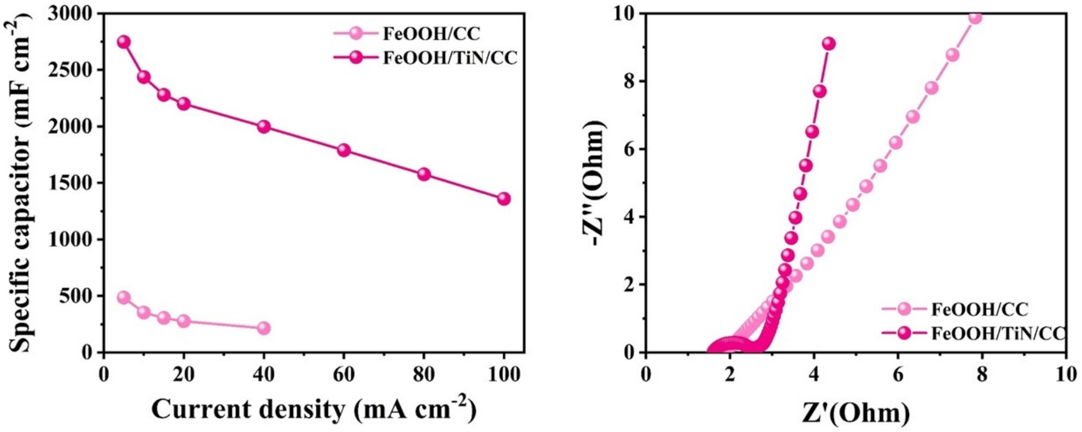

Fig. S28 Rate performance and EIS of FeOOH/CC and FeOOH/TiN/CC electrodes.

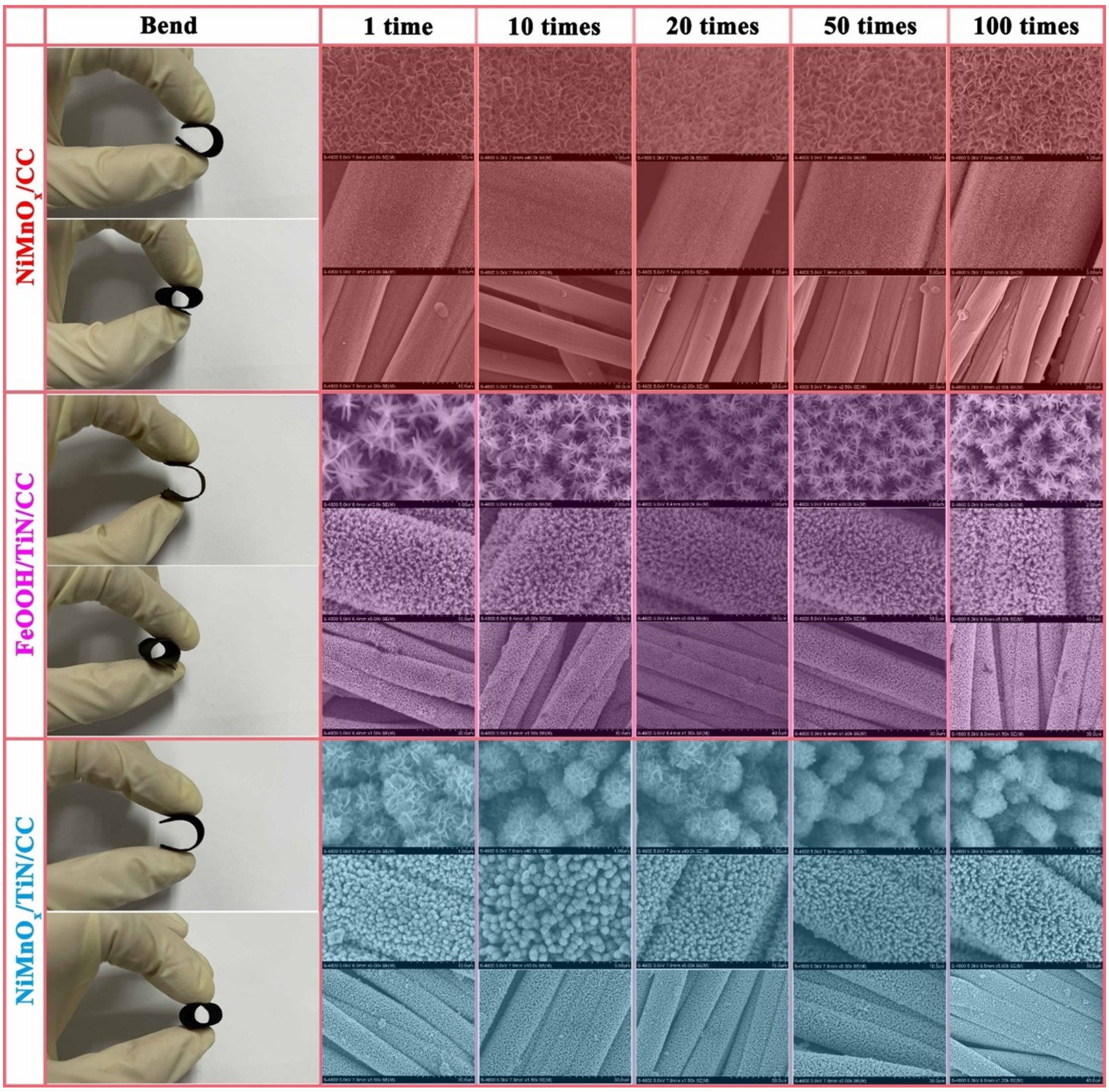

Fig. S29 Microstructure of $NiMnO_x$/CC, FeOOH/TiN/CC, and $NiMnO_x$/TiN/CC electrode materials during the continuous bending test

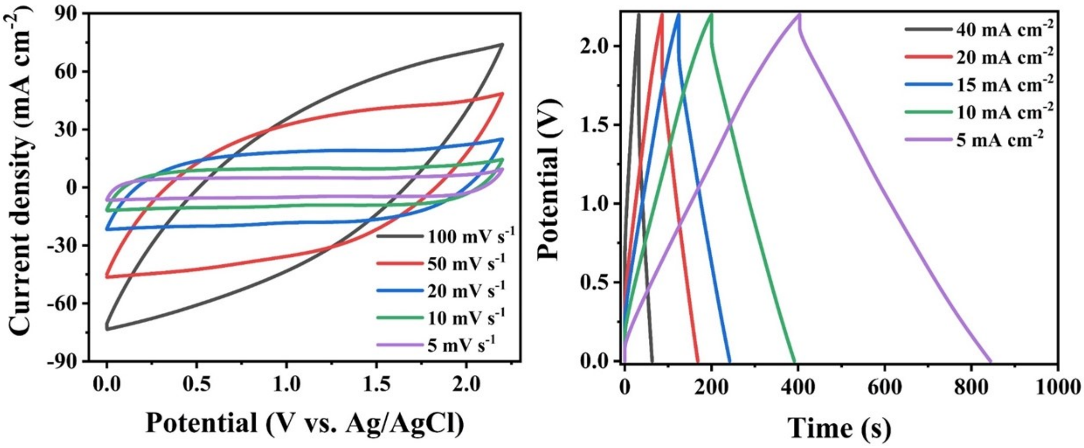

Fig. S30 CV and GCD curves of $NiMnO_x$/TiN/CC//FeOOH/TiN/CC flexible ASC device.

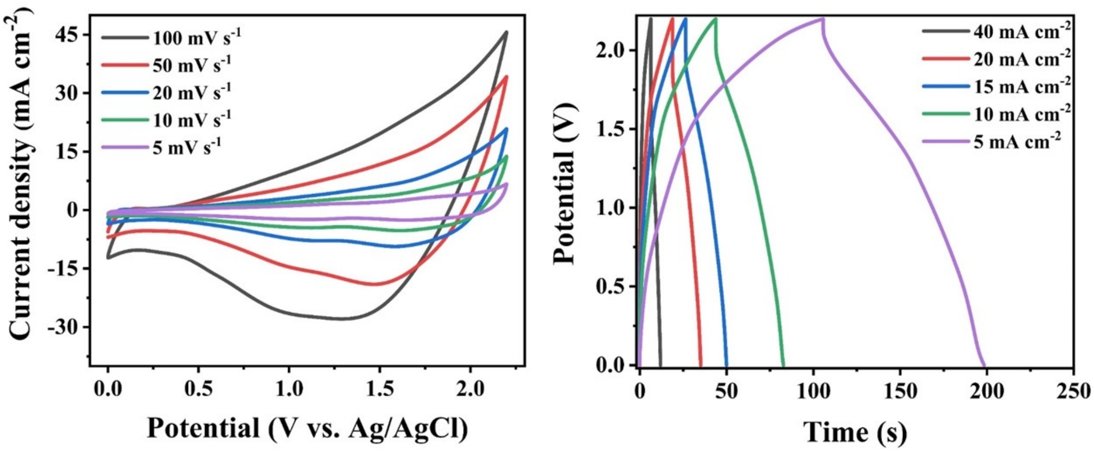

Fig. S31 CV and GCD curves of $NiMnO_x$/CC//FeOOH/CC flexible ASC device.

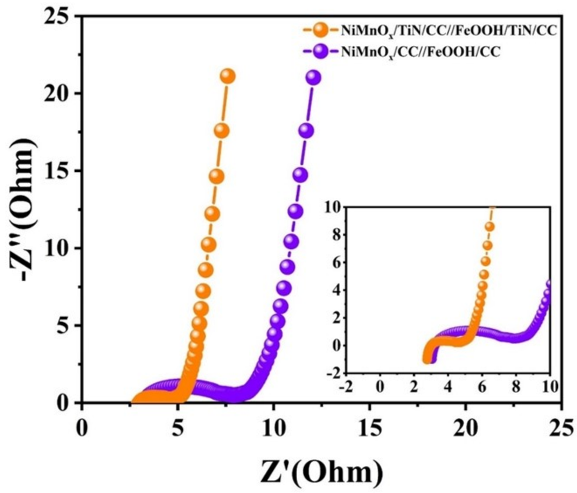

Fig. S32 EIS of NiMnO$_x$/TiN/CC//FeOOH/TiN/CC and NiMnO$_x$/CC//FeOOH/CC flexible ASC devices.

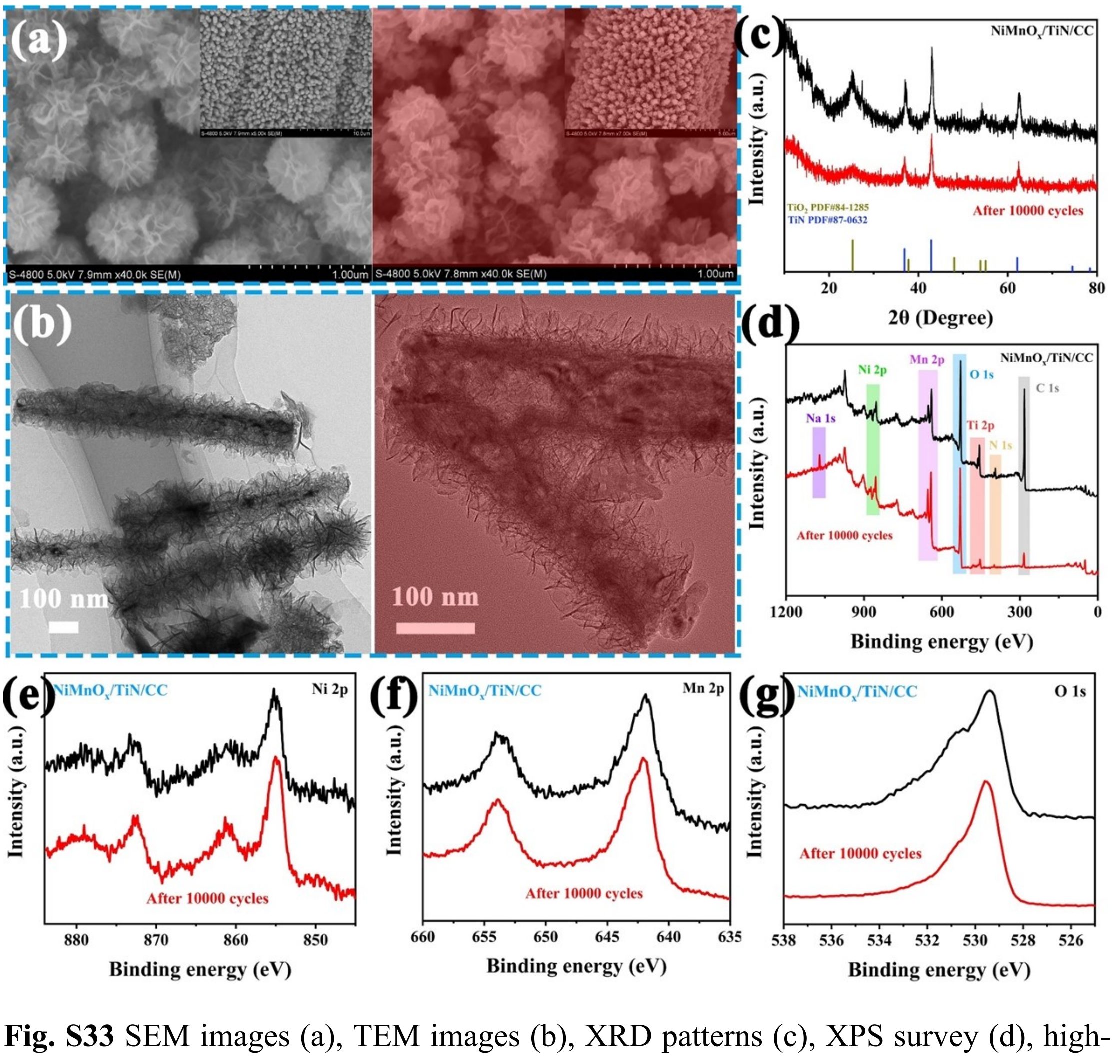

Fig. S33 SEM images (a), TEM images (b), XRD patterns (c), XPS survey (d), highresolution XPS spectra of Ni 2p (e), Mn 2p (f), O1s (g) for $NiMnO_x$/TiN/CC electrode before and after 10000 electrochemical cycles

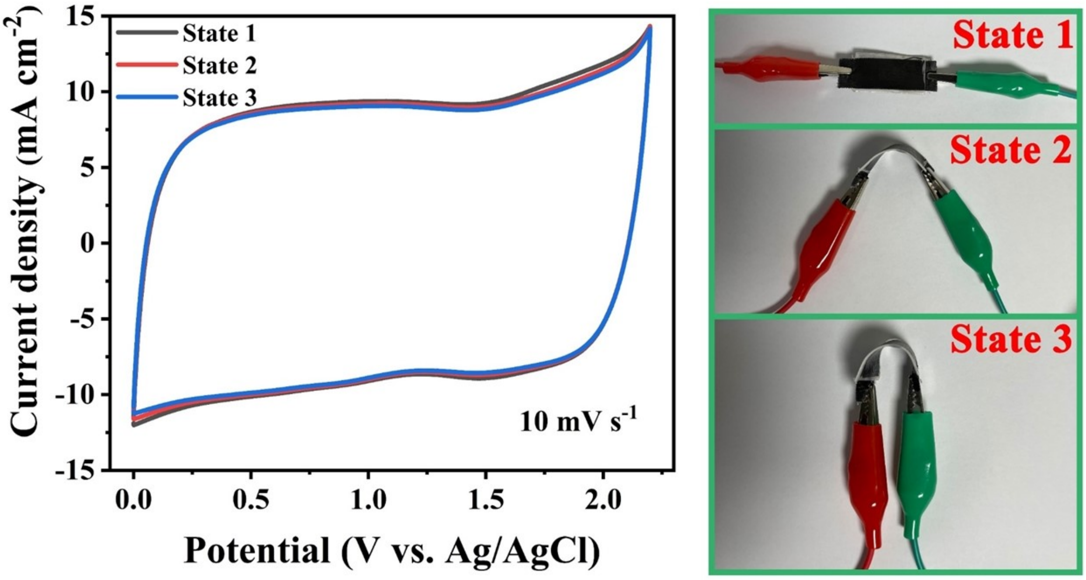

Fig. S34 Flexibility testing of flexible ASC devices.

S6. Supplementary Table S1-S9

Table S1 EDS test results of $NiMnO_x$/CC, $NiMn_2O_4$/CC, and $NiMnO_x$/TiN/CC electrode materials. (Unit: Atomic%)

Element	C	O	Ni	Mn	Ti	N
$NiMnO_x$/CC	10.29	59.52	9.84	20.35	\	\
$NiMn_2O_4$/CC	13.28	56.65	9.92	20.15	\	\
$NiMnO_x$/TiN/CC	6.28	49.39	10.74	21.58	6.26	5.75

Table S2 The areal capacitance of $NiMnO_x$/CC, $NiMn_2O_4$/CC and $NiMnO_x$/TiN/CC electrodes. (Unit: mF cm^{-2})

Current density	5 mA cm^{-2}	10 mA cm^{-2}	15 mA cm^{-2}	20 mA cm^{-2}	40 mA cm^{-2}	60 mA cm^{-2}	80 mA cm^{-2}	100 mA cm^{-2}
$NiMnO_x$-1.45	726.8	585.1	524.1	488.3	408.4	333.0	265.0	205.9
$NiMnO_x$-2.74	1201.6	958.9	844.4	768.0	582.7	419.8	292.5	185.7
$NiMnO_x$-5.12	1667.5	1335.3	1180.9	1065.1	701.2	394.8	182.2	78.1
$NiMnO_x$-8.98	2036.1	1431.1	981.7	670.8	188.4	\	\	\
$NiMn_2O_4$-1.42	427.4	366.01	324.9	297.3	247.7	223.2	183.8	143.7
$NiMn_2O_4$-2.18	624.9	522.1	457.7	411.1	328.5	277.2	205.5	166.0
$NiMn_2O_4$-5.07	1298.0	1081.6	959.5	869.7	713.24	622.7	506.2	412.7
$NiMnO_x$/TiN -1.66	921.3	800.4	741.3	707.9	634.8	584.2	546.4	516.6
$NiMnO_x$/TiN -4.38	2316.8	1949.2	1779.9	1671.45	1473.9	1337.1	1238.6	1157.6
$NiMnO_x$/TiN -5.58	2854.4	2489.1	2301.3	2193.5	1992.3	1824.3	1665.9	1485.7
$NiMnO_x$/TiN -10.12	4882.6	4104.5	3758.5	3579.4	3096.4	2667.1	2287.0	1935.2

Table S3 EDS test results of $NiMnO_x$/CC electrodes with different Ni to Mn atom ratios. (Unit: Atomic%)

Element	C	O	Ni	Mn
$NiMnO_x$/CC-1	12.19	44.26	7.88	35.68

$NiMnO_x$/CC-2	15.89	46.44	9.79	27.88
$NiMnO_x$/CC-3	6.17	51.37	19.79	22.67

Table S4 The areal capacitances of $NiMnO_x$/CC-1, $NiMnO_x$/CC-2, $NiMnO_x$/CC-3, NiO/CC, and MnO_2/CC electrodes. (Unit: mF cm^{-2})

Current density	5 mA cm^{-2}	10 mA cm^{-2}	15 mA cm^{-2}	20 mA cm^{-2}	40 mA cm^{-2}	60 mA cm^{-2}	80 mA cm^{-2}	100 mA cm^{-2}
$NiMnO_x$/CC-1	1638.7	1266.6	1048.0	933.2	621.4	391.8	285.7	190.8
$NiMnO_x$/CC -2	1517.1	1248.4	1084.1	956.3	606.8	413.9	240.2	150.5
$NiMnO_x$/CC -3	1541.5	1217.2	1060.0	946.1	617.3	345.9	202.6	121.4
NiO/CC	182.5	155.1	139.9	128.0	102.5	83.4	70.5	55.3
MnO_2/CC	1115.2	971.7	832.5	725.7	485.3	278.8	178.9	109.4

Table S5 The IR drop of $NiMnO_x$/CC, $NiMn_2O_4$/CC and $NiMnO_x$/TiN/CC electrodes. (Unit: V)

Current density	5 mA cm^{-2}	10 mA cm^{-2}	15 mA cm^{-2}	20 mA cm^{-2}	40 mA cm^{-2}	60 mA cm^{-2}	80 mA cm^{-2}	100 mA cm^{-2}
$NiMnO_x$-1.45	0.04	0.08	0.12	0.16	0.31	0.44	0.56	0.68
$NiMnO_x$-2.74	0.05	0.10	0.15	0.19	0.36	0.51	0.66	0.83
$NiMnO_x$-5.12	0.06	0.11	0.17	0.22	0.40	0.57	0.76	0.98
$NiMn_2O_4$-1.42	0.04	0.07	0.11	0.15	0.26	0.39	0.51	0.64
$NiMn_2O_4$-2.18	0.04	0.08	0.11	0.15	0.28	0.41	0.55	0.69
$NiMn_2O_4$-5.07	0.05	0.09	0.13	0.17	0.32	0.47	0.63	0.80
$NiMnO_x$/TiN -1.66	0.02	0.05	0.07	0.10	0.19	0.28	0.38	0.48
$NiMnO_x$/TiN -4.38	0.03	0.06	0.08	0.11	0.21	0.31	0.41	0.51
$NiMnO_x$/TiN -5.58	0.03	0.06	0.08	0.11	0.22	0.32	0.42	0.53

Table S6 Comparison of areal capacitance and rate capability of $NiMnO_x$/TiN/CC electrode with recently reported manganese oxide electrodes.

Electrode	Mass loading (mg cm^{-2})	Maximum areal capacitance	Minimum areal capacitance	Rate performance

$ZnO@MnO_2$ [1]	5.4	2280 mF cm^{-2} at 0.5 A g^{-1}	810 mF cm^{-2} at 10 A g^{-1}	0.5-10 A g^{-1} (20 times): 35.4%
MnO_2/CNT [2]	8.3	2800 mF cm^{-2} at 0.05 mV s^{-1}	1550 mF cm^{-2} at 0.8 mV s^{-1}	0.05-0.8 mV s^{-1} (16 times): 55.3%
3D graphene/CNT/MnO_2 [3]	8.4	730 mF cm^{-2} at 5 mV s^{-1}	90 mF cm^{-2} at 100 mV s^{-1}	5-100 mV s^{-1} (20 times): 12%
MnO_2/PEDOT [4]	8.6	800 mF cm^{-2} @ 4 mV s^{-1}	60 mF cm^{-2} at 100 mV s^{-1}	4-100 mV s^{-1} (25 times): 8%
MnO_2 /Graphene/Ni foam [5]	6.11	1500 mF cm^{-2} at 10 mV s^{-1}	450 mF cm^{-2} @ 100 mV s^{-1}	10-100 mV s^{-1} (10 times): 30%
3D graphene/MnO_2 [6]	9.8	1420 mF cm^{-2} at 2 mV s^{-1}	100 mF cm^{-2} at 100 mV s^{-1}	2-100 mV s^{-1} (50 times): 7%
Hierarchical Nanostructures MnO_2 [7]	10	3320 mF cm^{-2} at 1 mA cm^{-2}	1900 mF cm^{-2} at 30 mA cm^{-2}	1-30 mA cm^{-2} (30 times): 57.2%
MnO_2/Ni foam [8]	18	2700 mF cm^{-2} at 2 mA cm^{-2}	860 mF cm^{-2} at 20 mA cm^{-2}	2-20 mA cm^{-2} (10 times): 31%
MnO_x-h [9]	9	1610 mF cm^{-2} at 5 mV s^{-1}	618 mFcm^{-2} at 200 mV s^{-1}	5-100 mV s^{-1} (20 times): 38.4%
Mn_3O_4/MnOOH [10]	10	192.2 C g^{-1} at 1A g^{-1}	51.3 C g^{-1} at 20A g^{-1}	1-20 A g^{-1} (20 times): 26.7%
$NiMnO_x$/CC (this work)	**5.12 8.98**	**1667.5 mF cm^{-2} at 5 mA cm^{-2} 2036.1 mF cm^{-2} at 5 mA cm^{-2}**	**78.1 mF cm^{-2} at 100 mA cm^{-2} 188.4 mF cm^{-2} at 40 mA cm^{-2}**	**5-100 mA cm^{-2} (20 times): 4.7% 5-40 mA cm^{-2} (8 times): 9.3%**
$NiMnO_x$/TiN/CC (this work)	**5.58 10.12 10.12**	**2854.4 mF cm^{-2} at 5 mA cm^{-2} 4882.6 mF cm^{-2} at 5 mA cm^{-2} 4882.6 mF cm^{-2} at 5 mA cm^{-2}**	**1485.7 mF cm^{-2} at 100 mA cm^{-2} 3096.4 mF cm^{-2} at 40 mA cm^{-2} 1935.2 mF cm^{-2} at 100 mA cm^{-2}**	**5-100 mA cm^{-2} (20 times): 52.0% 5-40 mA cm^{-2} (8 times): 63.4% 5-100 mA cm^{-2} (20 times): 39.6%**

Table S7 The areal capacitance of $NiMnO_x$/CC, $NiMn_2O_4$/CC and $NiMnO_x$/TiN/CC symmetric supercapacitor devices. (Unit: mF cm^{-2})

Current density	5 mA cm^{-2}	10 mA cm^{-2}	15 mA cm^{-2}	20 mA cm^{-2}	40 mA cm^{-2}	60 mA cm^{-2}
$NiMnO_x$-5.12	485.65	322.02	215.92	134.90	\	\
$NiMn_2O_4$-5.07	95.30	64.96	47.86	36.77	\	\
$NiMnO_x$/TiN-5.58	1224.14	1160.99	1115.47	1086.46	935.69	779.15
TiN/CC	30.21	28.62	27.52	26.59	24.18	22.16

Table S8 The areal capacitance of FeOOH/CC and FeOOH/TiN/CC electrodes. (Unit:

mF cm^{-2})

Current density	5 mA cm^{-2}	10 mA cm^{-2}	15 mA cm^{-2}	20 mA cm^{-2}	40 mA cm^{-2}	60 mA cm^{-2}	80 mA cm^{-2}	100 mA cm^{-2}
FeOOH	484.4	352.4	304.4	275.8	213.9	\	\	\
FeOOH/TiN	2747.4	2436.3	2278.5	2199.1	1997.1	1788.6	1575.9	1359.2

Table S9 The areal capacitance of $NiMnO_x$/CC//FeOOH/CC and $NiMnO_x$/TiN/CC//FeOOH/TiN/CC electrodes. (Unit: mF cm^{-2})

Current density	5 mA cm^{-2}	10 mA cm^{-2}	15 mA cm^{-2}	20 mA cm^{-2}	40 mA cm^{-2}
$NiMnO_x$//FeOOH	215.6	184.6	171.2	161.3	120.4
$NiMnO_x$/TiN//FeOOH/TiN	1038.2	936.2	895.8	865.1	757.7

S7. References

[1] M. Huang, F. Li, X. L. Zhao, D. Luo, X. Q. You, Y. X. Zhang and G. Li, *Electrochim. Acta*, 2014, **152**, 172–177.

[2] L. Hu, W. Chen, X. Xie, N. Liu, Y. Yang, H. Wu, Y. Yao, M. Pasta, H. N. Alshareef and Y. Cui, *ACS Nano*, 2011, **5**, 8904–8913.

[3] J. Liu, L. Zhang, H. B. Wu, J. Lin, Z. Shen and X. W. Lou, *Energy Environ. Sci.*, 2014, **7**, 3709.

[4] Z. Su, C. Yang, C. Xu, H. Wu, Z. Zhang, T. Liu, C. Zhang, Q. Yang, B. Lia and F. Kang, *J. Mater. Chem. A*, 2013, **1**, 12432.

[5] T. Zhai, F. Wang, M. Yu, S. Xie, C. Liang, C. Li, F. Xiao, R. Tang, Q. Wu, X. Lu and Y. Tong, *Nanoscale*, 2013, **5**, 6790.

[6] Y. He, W. Chen, X. Li, Z. Zhang, J. Fu, C. Zhao and E. Xie, *ACS Nano*, 2013, **7**, 174–182.

[7] Z. H. Huang, Y. Song, D. Y. Feng, Z. Sun, X. Sun and X. X. Liu, *ACS Nano*, 2018, **12**, 3557–3576.

[8] J. Yang, L. Lian, H. Ruan, F. Xie and M. Wei, *Electrochim. Acta*, 2014, **163**, 189–194.

[9] Y. Song, T, Liu, B. Yao, M. Li, T. Kou, Z. H. Huang, D. Y. Feng, F. Wang, Y. Tong, X. X. Liu and Y. Li, *ACS Energy Lett.*, 2017, **2**, 1752–1759.

[10] W. Zheng, J. Halim, Z. M. Sun, J, Rosen and M. W. Barsoum, *Energy Storage Mater.*, 2021, **38**, 438–446.